Computing and Informatics, Vol. 40, 2021, 957–987, doi: 10.31577/cai_2021_5_957

DETECTION OF MACULA AND RECOGNITION OF AGED-RELATED MACULAR DEGENERATION IN RETINAL FUNDUS IMAGES

Sarmad Maqsood, Robertas Damaševičius

Department of Software Engineering
Kaunas University of Technology
Kaunas 51386, Lithuania
e-mail: sarmad.maqsood@ktu.edu, robertas.damasevicius@ktu.lt

Faisal Mehmood Shah

Pakistan Space and Upper Atmosphere Research Commission
Karachi 75270, Pakistan
e-mail: shahfaisal94@gmail.com

Rytis Maskeliūnas

Faculty of Applied Mathematics
Silesian University of Technology
Gliwice 44100, Poland
e-mail: rytis.maskeliunas@polsl.pl

Abstract. In aged people, the central vision is affected by Age-Related Macular Degeneration (AMD). From the digital retinal fundus images, AMD can be recognized because of the existence of Drusen, Choroidal Neovascularization (CNV), and Geographic Atrophy (GA). It is time-consuming and costly for the ophthalmologists to monitor fundus images. A monitoring system for automated digital fundus photography can reduce these problems. In this paper, we propose a new macula detection system based on contrast enhancement, top-hat transformation, and the modified Kirsch template method. Firstly, the retinal fundus image is processed through an image enhancement method so that the intensity distribution is

improved for finer visualization. The contrast-enhanced image is further improved using the top-hat transformation function to make the intensities level differentiable between the macula and different sections of images. The retinal vessel is enhanced by employing the modified Kirsch's template method. It enhances the vasculature structures and suppresses the blob-like structures. Furthermore, the OTSU thresholding is used to segment out the dark regions and separate the vessel to extract the candidate regions. The dark region and the background estimated image are subtracted from the extracted blood vessels image to obtain the exact location of the macula. The proposed method applied on 1349 images of STARE, DRIVE, MESSIDOR, and DIARETDB1 databases and achieved the average sensitivity, specificity, accuracy, positive predicted value, F1 score, and area under curve of 97.79 %, 97.65 %, 97.60 %, 97.38 %, 97.57 %, and 96.97 %, respectively. Experimental results reveal that the proposed method attains better performance, in terms of visual quality and enriched quantitative analysis, in comparison with eminent state-of-the-art methods.

Keywords: Medical image processing, contrast enhancement, macula detection, retinal fundus image, blood vessels segmentation

Mathematics Subject Classification 2010: 68U10

1 INTRODUCTION

Age-related Macular Degeneration (AMD) is a general cause of blindness for people aged 55 or above all over the world [1, 2]. There were about 450 million people with diabetes in 2016, and this number is anticipated to increase to 2 billion people by 2050 because of the increase in the aging population [3]. The most common problem of diabetes is diabetic retinopathy (DR), which is the main cause of visual loss and blindness [4]. The patients of diabetes with DR range from 21.9 % to 36.8 % [5].

A large amount of the world's health budget requires proper diagnosis, screening, and analysis of the diseases. DR can be curable, appreciable, and can gain the vision back only when the proper medication begins from the initial stage of the disease, however, no efficacious cure is currently accessible to gain the vision back once it is growing. Hence, the proper treatment at the early stage can recover the vision [6, 7, 8]. In many growing countries, there is a scarcity of ophthalmologists, and the number of people aged 58 and above is increasing at a double rate in relation to the number of medical specialists in developed countries [9].

Ophthalmologists are required to assess the alterations in the retina over time for the early detection and inspection of the development of the disease. Manual inspection of the development of the disease is almost unimaginable by the specialist in such a large population, which has become especially relevant considering the current COVID-19 pandemic and associated lockdowns. Therefore, now it is deemed

necessary to make the process automated and retain track of the alterations of the retina [10, 11]. Today, from the retinal fundus camera images the retina containing pathologies for instance drusen in the digital image can easily be seen [12].

A macula is an essential unit of the retina in the human eye which manages sharp central vision [13]. The macula is a yellowish oval shape situated on the secular side of the optic nerve head close to the center of the retina. It consists of high visual acuity. It performs the blockage of the natural sunlight because it can consume the extra blue and ultraviolet light, which enters the human eye. The damage in the macula and any other abnormalities like red lesions, cotton wool spots, and exudates nearby macula result in the central vision loss. The continuous damage of a macula or the existence of hard exudates nearby the macular area is an eye disease identified as clinically significant macular edema (CSME) [14].

Macula recognition is essential in discovering and diagnosing eye-related pathologies [15] such as diabetic retinopathy [16]. Firstly, image processing algorithms are important in reducing human errors, secondly, the early detection of eye disease assists in averting costly laser surgery, and thirdly, this helps in comparison of many fundus images at an instant. To enhance the medical treatment this type of observation is very significant. The ophthalmologists need time to identify the disease in the human eye retina, they can detect the disease, but it is expensive as well [17]. It is also not possible to detect manually. Hence taking these problems in line that are challenged in the medical imaging field.

For the rapid examination and cure of numerous eye diseases, the retinal fundus photographs are generally used in clinics [18]. The fundus photography can be achieved by the fundus camera that consists of a low power microscope with a close camera. Retinal fundus image demonstrates the internal surface of the human eye which comprises the macula, fovea, optic disc, retinal blood vessels, optic cup, posterior pole, and veins. The colored fundus image of the human eye is displayed in Figure 1, which labels important features like macula, optic disc, blood vessels, etc. These are some basic features of the fundus image that assist in evaluating the pre-processing step.

Although existing methods achieved good performance in the segmentation of retinal vessels and detecting the macula, however, the accurate automatic detection of the macula and the segmentation of the retinal vessel is still a challenging task due to variations in the color, shape, and size of the macula. The limitations of the existing methods can be summarized as follows:

1. Failed identification of the thin retinal vessels with poor contrast.
2. Poor segmentation of the retinal vessel appears to distort edges due to the influence of noise and other uneven contrast artifacts, crossing the regions and the regions of the close vessels.
3. Blurring effect near the strong edges during the localization of the macula.
4. Most of the existing methods are computationally complex and take a longer processing time to detect the macula.

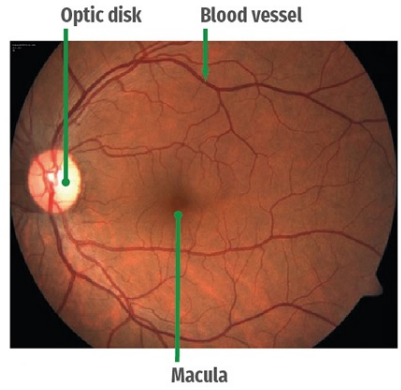

Figure 1. Colored fundus image with important features [3]

We propose a novel automatic detection method of macula and identification of the AMD disease using retinal fundus images, having the following contributions.

1. We apply contrast stretching as a preprocessing step to improve the edge details from the input source images.
2. We propose a modified Kirsch's template method for the segmentation which is used to divide the vessel to extract the candidate regions.
3. The novel shaped based extraction technique is used to detect the location of the macula.
4. The computational efficiency of the proposed method is also assessed. The proposed method takes less processing time to detect the location of the macula when compared with existing algorithms.
5. Furthermore, this simulation analysis indicates that the proposed method achieves better performance, both visually and provides improved information extraction, in comparison with existing methods, as it will be debated in Section 4.

The remaining paper is structured as follows. Section 2 reviews the prominent related work on macula detection. In Section 3 the detailed methodology of the proposed method is discussed. Section 4 analyses the performance of the proposed method in comparison with the other state-of-the-art methods and, finally, Section 5 concludes this paper with future research goals.

2 RELATED WORK

This section critically reviews the significant work on retinal vessel segmentation and macula detection using the retinal fundus images.

Many researchers have worked on the automated detection of the macula using retinal fundus images. Nazari et al. [19] proposed a hybrid of multi-scale detection

with top-hat transformation pre-processing to enhance the contrast of the vessel from the background for blood vessel segmentation. The method achieved 95.10 % accuracy on the DRIVE dataset. Alais et al. [15] presented an algorithm based on a fully convolutional network for the recognition of macular region and fovea using retinal fundus image. The authors selected 6098 retinal fundus images from e-ophtha database [17] and obtained an accuracy of 96.4 %. Syed et al. [18] proposed an automatic system for the detection of Macular Edema (ME) using retinal fundus images. This method uses different hybrid features and support vector machines (SVM) for the identification of fovea and exudates segmentation which further classify the ME. This method uses public and local databases and attained an accuracy of 96.1 %. GeethaRamani and Balasubramanian [20] use a data mining approach to segment out the macula. An unsupervised heuristic-based clustering method creates the binary image which is further post-processed to remove the undesirable components to detect the macula. This method was tested on HRF, DRIVE, DIARETDB0, DIARETDB1, HEI-MED, STARE, and MESSIDOR datasets and obtained the accuracy of 100 %, 100 %, 96.92 %, 97.75 %, 98.81 %, 90 %, and 99.33 %, respectively. Orujov et al. [21] proposed a system based on fuzzy rules for the detection of blood vessels in the retinal fundus images. The experiments were examined on DRIVE, STARE, and CHASEdb datasets and obtained an accuracy of 0.939, 0.865, and 0.950 respectively. Saroj et al. [22] presented a method based on Frechet matched filter for the segmentation of retinal vessels and obtained the specificity of 97.24 %, the sensitivity of 72.78 %, and accuracy of 95.09 % for the STARE database. Ghoshal et al. [23] use retinal fundus images for vessel extraction by removing the noise to get the segmented vessels. The experiment was performed on a the DRIVE dataset and attained a sensitivity of 0.7260, specificity of 0.9802, and accuracy of 0.9563. Dharmawan et al. [24] developed an automated segmentation of optic disc using retinal fundus images. The modified Dolph-Chebyshev Type II matched filter is used to detect the boundaries of the optic disc. This method uses the DRIVE and MESSIDOR databases with an average accuracy of 99 %. Kaya [25] presented an algorithm for optic disk (OD) detection by employing the Cuckoo Search method and structural similarity index measure (SSIM) using retinal images. This method has an accuracy of 100 % on ONHSD, 100 % on DRIONS, and 97.5 % on DRIVE databases. Palanivel et al. [26] proposed segmentation of retinal vessels images using a supervised classification approach. The retinal vessels are segmented using multifractal characterization. This method uses the DRIVE, STARE, and CHASEDB1 databases and attained an average accuracy of 0.9542, 0.9459, and 0.9459, respectively. Kadry et al. [27] designed a Multi-Scale-Matched-Filter (MSMF) using the Slime-Mould-Optimization algorithm to extract blood vessels from digital fundus images. Then, an examination among extracted vessels and the Ground-Truth image is executed and the Image-Performance-Values are computed for images, achieving an accuracy of 97.15 % on DRIVE and 97.16 % on CHASE_DB1 datasets. Agurto et al. [28] proposed the automatic approach for the detection of the macula in the fundus images using a multi-scale optimization technique. Finally, Aljazaeri et al. [29] proposed a deep learning approach for glaucoma detection in retinal fundus images.

They used a faster region proposal neural network (RCNN) to detect the optical disc. Then a regression network was trained to estimate the cup-to-disc ratio by analyzing reign around the optical disc, and the MESSIDOR dataset was used for validation.

From the literature review, the previous methods have provided better information extraction. Although, there are still various concerns that need serious attention, such as

1. poor contrast when identifying the retinal vessels,
2. low segmentation of the retinal vessel due to influence of noise, and
3. blurring effect near the strong edges during the localization of the macula.

To resolve these aforementioned problems, we propose a novel macula detection method that is elaborated on in the following section.

3 THE PROPOSED TECHNIQUE

The schematic flowchart of the proposed method is displayed in Figure 2. Firstly, a contrast enhancement-based technique is employed on the retinal fundus image to enhance the contrast. To refine the quality of the image for perfect segmentation, a pre-processing step is applied to the source images. Morphological filtering is employed on the pre-processed image to enhance the retinal vasculature of the fundus image. After that, segmentation is applied to the pre-processed color fundus images. Segmentation is employed to separate the vessel to extract candidate regions. For the exact detection of the macula, the image contains both the vessel and macula combined and the background image should be estimated, therefore it will be easy to get the macula by subtracting these images from the filtered image. The image not only contains the macula but also consists of some broken vessel parts. The location of the macula is necessary, hence the radius and the diameter of the centroid and eccentricity of connected components are computed. By computing these many features are extracted in which location of the macula can easily be recognized. Recognition of the normal and the AMD diseases of the eye can be differentiated by determining the shape of the macula if the shape of the macula is found around it is classified as normal and if a shape is not round it is categorized as AMD. The result is also verified by the ophthalmologist.

3.1 Green Channel Extraction

Colored retinal fundus images are in imperfect contrast. Therefore, it is very important to enhance the contrast of the images. To find the exact location of the macula the color images are converted into the green channel. To figure out the luminance data of the color images after reducing hue and saturation, a grey-scale strategy has been applied. The extreme local contrast among the background and foreground can be found by extracting the green channel of the color images. The

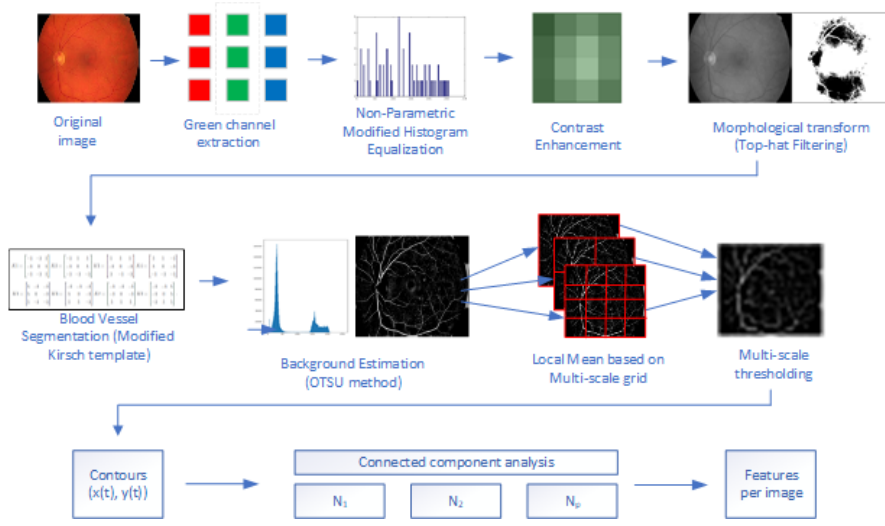

Figure 2. Schematic diagram of the proposed system

Green channel captures the great intensity contrast between the macula and the background. Retinal fundus images need to be separated into three channels and we use only one of them.

The extraction of red, blue, and green channels of the retinal fundus image is shown in Figure 3. As shown in Figures 3 a) and 3 b), the red and blue channels are not extracting complete information. The blue channel extracted from the retinal images has poor contrast and does not contain all the necessary information for further processing. In the red channel, the vessels in the fundus images are found out noticeable, on the other hand, the red channel incorporates much noise or sometimes it is just saturated. In Figure 3 c) green channel provides a full and detailed information of the retinal fundus image. Green channel extraction from the color retinal images provides a prominent outcome in the contrast of blood vessels as in this channel it darkens the blood vessels on a bright background. So, in this paper, we have used the green channel for the exact localization of macula and the detection of AMD.

3.2 Contrast Enhancement

To enhance the low contrast images the histogram equalization approach seems to be a more effective technique. The source image can be delineated as close as possible to the uniform distribution in the histogram equalization method. Non-Parametric Modified Histogram Equalization (NMHE) [30] is used to improve the contrast and keep the average brightness of the input image.

First, NMHE eliminates the spikes from the original histogram. After that, the

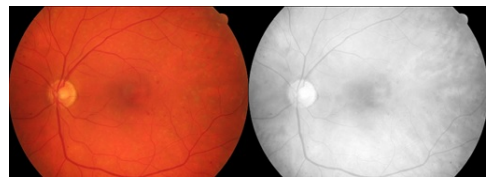

a)

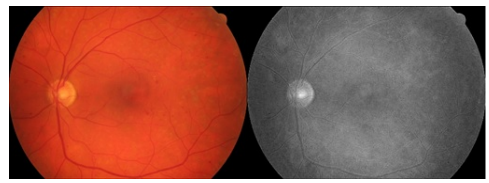

b)

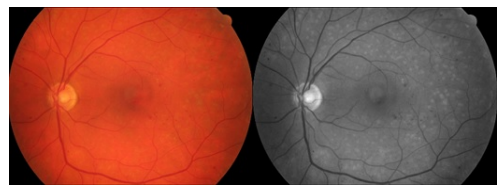

c)

Figure 3. Left: The retinal fungus image. Right: a) Red channel extraction, b) Blue channel extraction, c) Green channel extraction.

algorithm clipped the histogram and calculated the cumulative distribution function (CDF) of the transitional renewed histogram from the uniform one. It operates as a weighting factor to build a final updated histogram. Equation (1) determines a threshold and pixels higher than the threshold contribute in the modified histogram as follows:

$$A_m(i) = f[i \mid B], \tag{1}$$

where $f[i \mid B]$ is the occurrence probability of i^{th} intensity-level given horizontal contrast variation B. A measure of un-equalization (M_e) is calculated in Equation (2).

$$M_e = \sum (e - h_m c). \tag{2}$$

The value of M_e is a pointer to those images which do not follow a uniform distribution. e is a uniform probability density function (PDF), and $h_m c$ is a modified clipped histogram calculated from the original histogram. The weighted factor of the modified PDF is given in Equation (3).

$$h_N = (M_e)A_m + (1 - M_e)e. \tag{3}$$

The CDF of the image is achieved from redesigned histogram h_N as in Equa-

tion (4).

$$r_N(s) = \sum_{i=0}^{s} h_N(s). \tag{4}$$

The transformation operation $X(m)$ obtained by using r_N is given in Equation (5).

$$X(m) = [(Q-1)r_N(s) + 0.5], \tag{5}$$

where $X(m)$ is employed to green channel extraction images to obtain the contrast-enhanced images. Contrast enhancement results in improved edges in the input images.

Figures 4 a) and 4 b) show the enhancement from the green channel and the contrast-enhanced image, respectively. From the images, it can be observed that after applying the contrast enhancement method, the image gradients are greatly enhanced. On completion of this phase, the proposed method enters the third stage, which is elaborated in the below subsection.

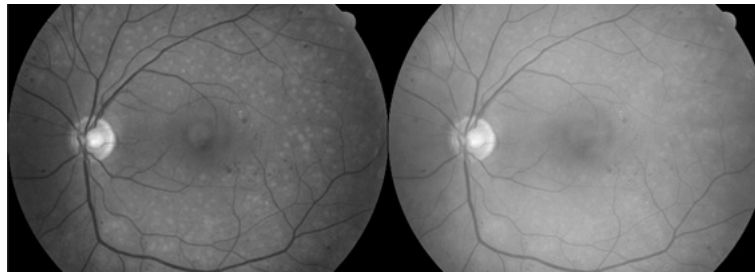

a) Enhancement from green channel

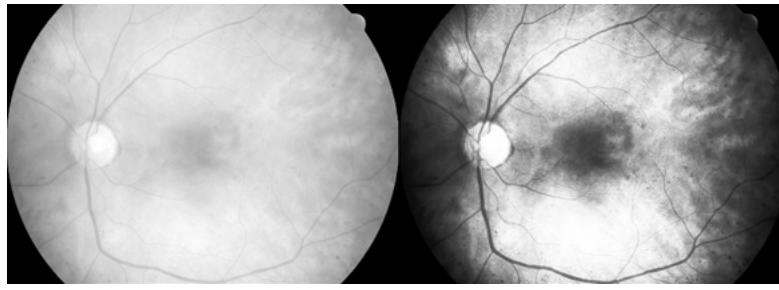

b) Final contrast enhancement

Figure 4. The retinal fungus image for contrast enhancement

3.3 Top-Hat Filtering

Contrast enhancement based techniques enhance the image quality, but still, the images need more enhancement to protrude dark objects in the retinal fundus im-

ages. The blood vessels and macula have dark intensities so for the detection of the macula, the contrast-enhanced images need more modification to darken the dark intensity objects in the fundus images. Blood vessels, hemorrhages, and macula are the darker objects in the retinal fundus image, by implementing a top-hat filter, the image gets clear from the dark objects. Therefore, there is a clear intensity separation between the darker segment and brighter segment and hence can easily get the vessels and macula from an image.

The top-hat transform of the function m is expressed in Equation (6) as:

$$X_h(m) = m \bullet h - m \tag{6}$$

where $\bullet$ denotes the closing operation.

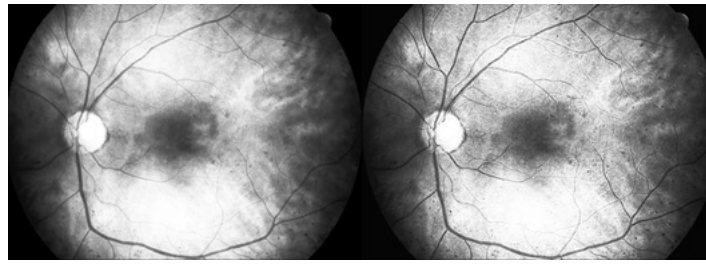

Figure 5. Illustration of top-hat filtering: original image (left), filtered image (right)

After top-hat filtering, the proposed method enters the fourth stage, which is discussed in the next subsection.

3.4 Segmentation of Blood Vessel

In this section, the retinal blood vessels are obtained by using the modification to the legacy Kirsch's template technique [31]. Blood vessel extraction is the most important part in diagnosing the eye disease in fundus image [32]. The modified Kirsch templates use the size of 3×3 kernels for the extraction of blood vessels when the threshold value reaches the maximum. This method is commonly used to cognizance the edges and extract blood vessels [33, 34]. The result of using the Kirsch model is to obtain the image with clear blood vessels. Blood vessel detection material-specific and mark pixels are verified by defining the brightness level of neighboring pixels. The blood vessel extraction is achieved by observing the brightness level change in the image, if there is no brightness difference then there is no probability of blood vessels. The modified Kirsch template for the extraction of the blood vessel is executed using the single mask of size 3×3 and rotate it in

45-degree increments via all the 8 direction Kirsch convolution kernels as:

$$K1 = \begin{bmatrix} -3 & -3 & 5 \\ -3 & 0 & 5 \\ -3 & -3 & 5 \end{bmatrix}, \quad K2 = \begin{bmatrix} -3 & 5 & 5 \\ -3 & 0 & 5 \\ -3 & -3 & -3 \end{bmatrix}, \quad K3 = \begin{bmatrix} 5 & 5 & 5 \\ -3 & 0 & -3 \\ 3 & -3 & -3 \end{bmatrix},$$

$$K4 = \begin{bmatrix} 5 & 5 & -3 \\ 5 & 0 & -3 \\ -3 & -3 & -3 \end{bmatrix}, \quad K5 = \begin{bmatrix} 5 & -3 & -3 \\ 5 & 0 & -3 \\ 5 & -3 & -3 \end{bmatrix}, \quad K6 = \begin{bmatrix} -3 & -3 & -3 \\ 5 & 0 & -3 \\ 5 & 5 & -3 \end{bmatrix},$$

$$K7 = \begin{bmatrix} -3 & -3 & -3 \\ -3 & 0 & -3 \\ 5 & 5 & 5 \end{bmatrix}, \quad K8 = \begin{bmatrix} -3 & -3 & 5 \\ -3 & 0 & 5 \\ -3 & 5 & 5 \end{bmatrix}.$$

The magnitude of the blood vessel is calculated by employing the modified Kirsch operator where maximum magnitude exists along with all the directions. The Kirsch convolution kernel matrix has all the information regarding the pixel and its neighbors. It detects all the blood vessels in all directions. The modified Kirsch template model has eight feasible directions that include north, west, south, east, northeast, southeast, southwest, and northwest. From all the possible constructed templates, the template having the largest value is considered as the output value and then the blood vessel is extracted accurately. For the exact extraction of blood vessels, the Kirsch template can arrange and rearrange the threshold values to get the accurate blood vessel [35].

The modified Kirsch operator $Z(x)$ for the detection of blood vessels is expressed in Equation (7) as:

$$Z(x) = \max[1, \max_{k} \sum_{k-1}^{k+1} X_h(m)], \tag{7}$$

where $X_h(m)$ is used for all the eight neighbouring pixels to x and subscripts k is calculated by modulo eight. In eight different directions, the modified Kirsch template method uses the spatial filters. This completes the blood vessels segmentation phase and allows the proposed method to continue to the following subsection.

3.5 Estimation of Background and Black Objects Segmentation

To get the macula the background image needs to be estimated by subtracting this image from the modified Kirsch template image. The region of interest (ROI) is the dark region because vessels and macula both appear dark in the enhanced image. In this step, images need to be binarized for removing the small objects or filling small holes. For the computing or manipulative, the object features that include size or intensity mean, binary object masks can be used [36]. In retinal fundus images, numerous spots include hemorrhages, macula, optic disc, and vessels. These spots are different from each other according to their size, color, and shape. The algorithm

a) Original image b) Extracted blood vessels

Figure 6. Extraction of blood vessels using the modified Kirsch template method

for the feature extraction from the enhanced image using the OTSU method is displayed in Figure 7.

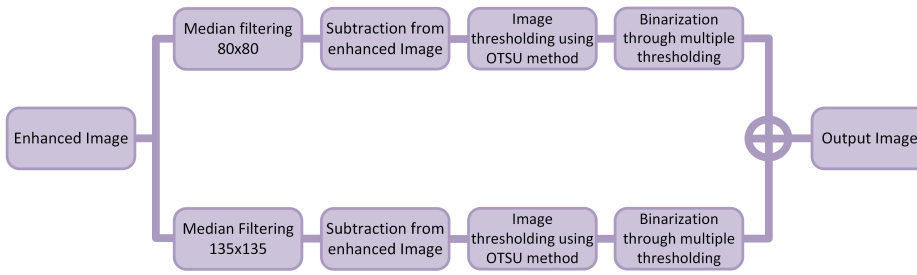

Figure 7. Flow diagram for feature extraction

A multi-scale segmentation method is used to segment the macula and vessels. Then a median filter [37] is applied with different sizes according to the size of macula and vessel to smoothen the image and then subtract from the enhanced image, after applying median filter the dark regions look brighter and more segmented using the OTSU method. For the removal of bright spots, the image having negative pixels is fixed to zero. For the detection of the macula with thin and thick vessels, a multi-scale thresholding method is used. The sizes for the median filter are selected as 80×80 and 135×135, the final image is obtained by joining the estimated images from these filters.

A median filter is used to eliminate the separated pixels and some small areas produced by the image noise. The median filter lies in the middle of the observation data. It minimizes the $l1$ norm in Equation (8) as:

$$M(x) = \sum_{i=1}^{n} |Z(x) - \text{Med}| \longrightarrow \min. \tag{8}$$

To acquire the updated binary image, the median filtered image is then sub-

tracted from the source image in Equation (9).

$$S(x) = A_m(i) - M(x). \tag{9}$$

Then the OTSU method [38] is used for the segmentation and binarization of retinal fundus images. As a result, the thin and thick vessels in the binary image are acquired. Finally, image addition is used to create a double exposure of two images into a single image. The final image is obtained by combining two binary images. The resultant image of the estimation of background and black objects segmentation is shown in Figure 8. This completes the estimation of background and black objects segmentation phase that leads the proposed method to continue to the next stage, which is discussed in the next subsection.

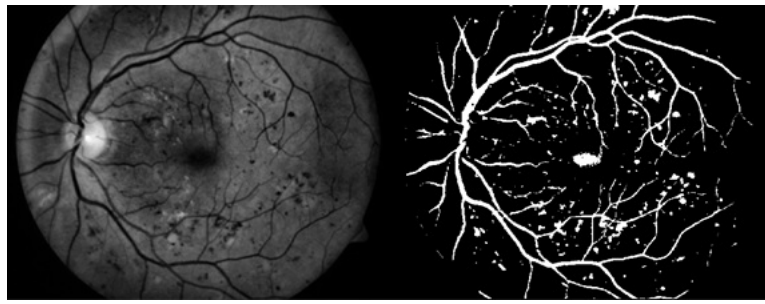

a)

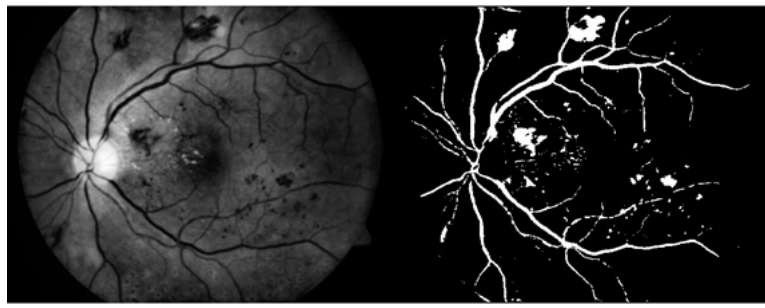

b)

Figure 8. Estimation of background and black object segmentation

3.6 Detection of Macula Using Shape Based Extraction Technique

Finally, the macula is detected by subtracting the background estimated image from the filtered image. The size of macula is 3mm and oval-shaped, having clear edges and dark in color. The resultant image contains all objects on retinal images with dark intensities that include hemorrhages, blood vessels, some sort of noise, broken

vessels, and the macula. To compute and extract the macula from this resultant image, we need to calculate the radius and diameter of the centroid and eccentricity of connected components. The steps of level 1 extraction are illustrated as follows.

1. Computation of the connected components from the image which is obtained by subtraction of the modified Kirsch's template method image and background estimated image.
2. Extraction of centroids from connected components and calculation of their centers.
3. Compute the number of centroids.
4. Find the major and minor axis length of centroids and then subtract them.
5. If the subtracted value is less than 30 than the detected object is macula because major axis and minor axis are longest and shortest diameter if both are equal than the subtracted value will be zero, then the object will be circular as the subtraction value is less than the object is similar in blob shape.

The detection of the macula is also detailed in Algorithm 1.

Algorithm 1 Extraction of Macula

Input Image: Image as a result of subtracted modified Kirsch's template method and background estimated image.
Output Image: Macula candidate image.
begin
stat = regionprob(image)
centre = stat.centroid
l = length(centre)
data = major axis length centroid-minor axis length centroid
for $i = 1 : l$ **do**
begin
if data < 30 **then**
calculate diameter and radius of centroid
radius[i] = radius
else
radius[i] = 0
end if
end for
end

After completing the macula detection stage, the proposed method enters the final stage, which is presented in the next subsection.

3.7 Categorization of Normal and AMD Case Macula

As we can see from Figures 9, 10, 11, the localization of macula has been detected significantly using the proposed method. The size of the macula is 3 mm, having dark color, round in shape with clear edges. If the macula lies under the given condition, the subjected image is considered as a healthy eye; otherwise, the corresponding retinal image is considered as age-related macular degeneration (AMD) eye.

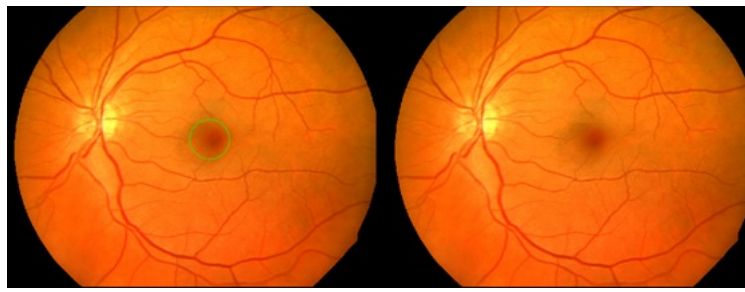

a) Color image

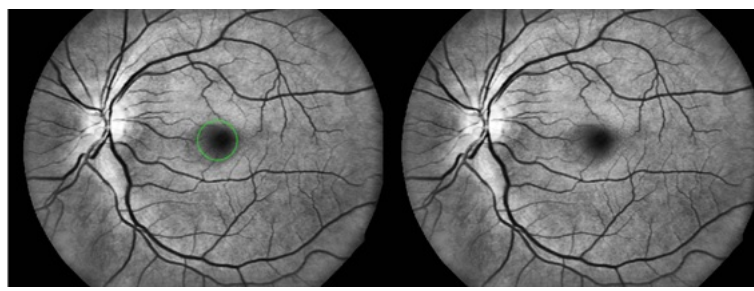

b) Enhanced image

Figure 9. Localization of macula on retinal fundus image. Location of macula is shown by green circle.

This section completes the macula detection process through our proposed method. The next section details the experimental results and presents a discussion of our proposed method.

4 PERFORMANCE EVALUATION

4.1 Simulation Setup

The proposed system is compared with some of the other techniques to clarify the efficacy and the perfection of the algorithm. The experiments are executed on a laptop in Matlab R2020b (MathWorks Inc.) and on an Intel(R) Core(TM) i7

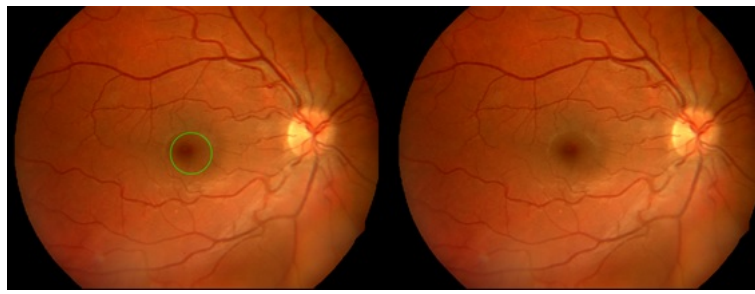

a) Color image

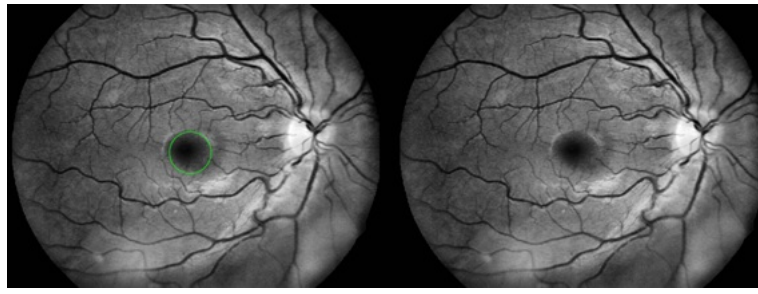

b) Enhanced image

Figure 10. Localization of macula of normal eye fundus image

2.6 GHz processor with 12 GB RAM. The performance of the proposed method is verified on the DRIVE [39], STARE [40], MESSIDOR [41], and DIARETDB1 [42] datasets for the detection of macula. In this experiment, a total of 1 349 images are used, in which 40 images are taken from the DRIVE dataset, 20 images from the STARE dataset, 1 200 images from the MESSIDOR dataset, and 89 images from the DIARETDB1 dataset. The resolution of the DRIVE dataset is 565×584, STARE dataset is 700×605, MESSIDOR and DIARETDB1 dataset is $1\,440 \times 960$. Table 1 shows a complete description of all used datasets.

Database	**Number of Images**	**Normal**	**AMD**
DRIVE	40	33	7
STARE	20	12	8
MESSIDOR	1 200	971	229
DIARETDB1	89	5	84
Total Images	1 349	1 021	328

Table 1. Complete description of database

The dataset contains the retinal fundus images of healthy eyes, having hemorrhages, hard and soft exudates, AMD disease, diabetic retinopathy, noise artifacts, and many more imperfections that are considered very common to low-cost fundus

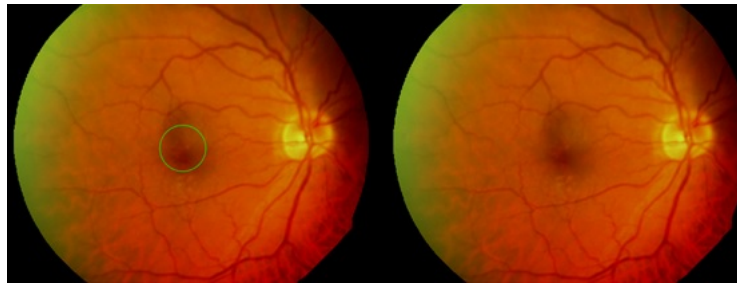

a) Color image

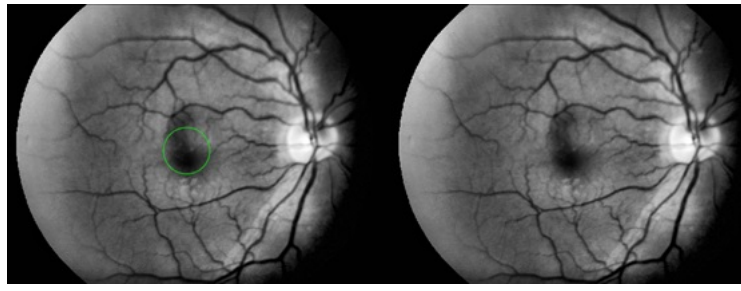

b) Enhanced image

Figure 11. Localization of macula of macular degeneration (AMD) eye image

images, therefore, the proposed method is designed to remove these difficulties with slight modifications. Figure 12 shows the retinal fundus image for the normal and the AMD eye.

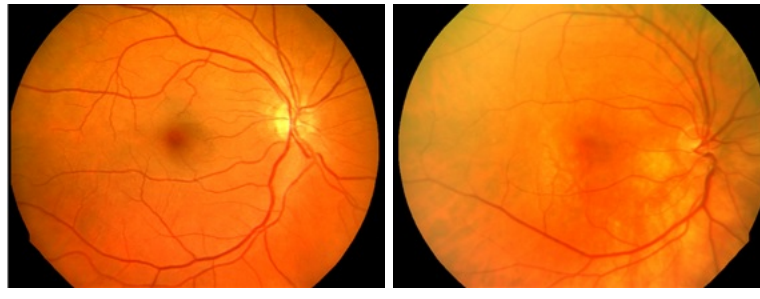

a) Normal eye b) AMD eye

Figure 12. Retinal fundus image

4.2 Extraction of Macula for Normal and AMD Eye

The proposed method is evaluated using publicly available datasets. The complete database of 1 349 retinal fundus images was taken as a set and none of them is excluded. In addition to visual inspection, the quantitative comparison is done by comparing the ground truth and the macula detected method. Firstly, all the 1349 images of the complete database were perfectly pre-processed. In this subsection, the results of the proposed method are presented in identifying the macula. Figures 13 and 14 show the results of extraction of the macula for the normal and the AMD eye classes of fundus images.

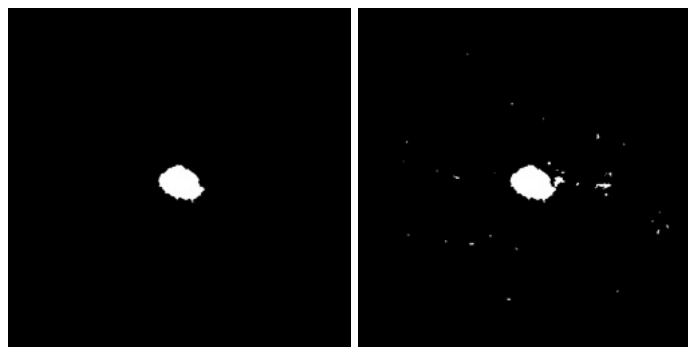

a) Enhanced retinal image b) Extraction of macula

Figure 13. Normal retinal fundus image

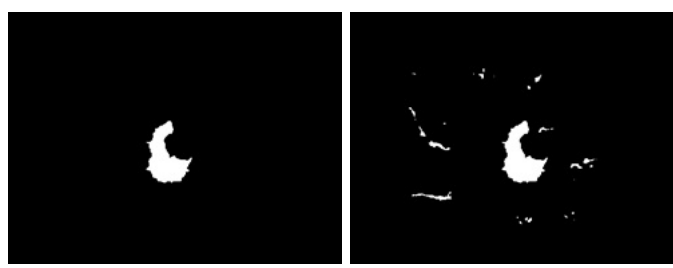

a) Enhanced retinal image b) Extraction of macula

Figure 14. AMD retinal fundus image

Figures 15 and 16 show the localization of the macula in the enhanced image for the normal and the AMD eye.

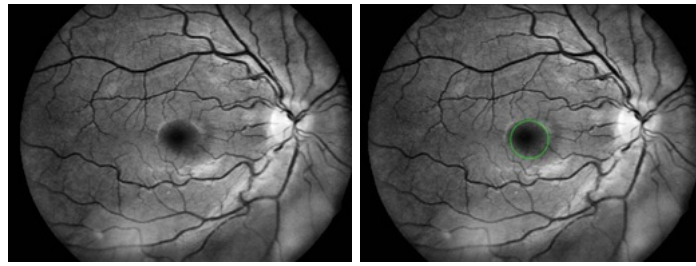

a) Enhanced retinal image b) Localization of macula

Figure 15. Normal retinal fundus image

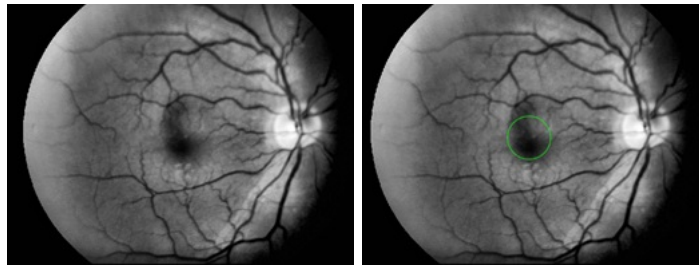

a) Enhanced retinal image b) Localization of macula

Figure 16. AMD retinal fundus image

4.3 Performance Evaluation Criteria

The results of our proposed method are analysed using several metrics, i.e., Accuracy (Acc), Sensitivity (Sn), Specificity (Sp), Area under Receiver Operating Characteristic (ROC) curve also known as Area Under Curve (AUC), Positive Predicted Value (PPV) and F1 score ($F1$). These parameters are used for the measurable factor to compare the performance of the proposed method with other methods. These metrics are defined as follows:

$$Accuracy(Acc) = \frac{(TP + TN)}{(TP + FP + TN + FN)} \times 100\,\%, \tag{10}$$

$$Sensitivity(Sn) = \frac{TP}{(TP + FN)} \times 100\,\%, \tag{11}$$

$$Specificity(Sp) = \frac{TN}{(TN + FP)} \times 100\,\%, \tag{12}$$

$$PPV = \frac{TP}{(TP + FP)} \times 100\,\%, \tag{13}$$

$$F1\ score\ (F1) = 2 * \frac{Precision * Recall}{Precision + Recall}. \tag{14}$$

Accuracy shows the localization of macula and detection of normal and abnormal cases. Sensitivity shows the effectiveness in the identification of the actual macula. Specificity indicates the non-macula candidates. In the equations TP are True Positive values which mean images containing the macula that are AMD, TN are True Negative values that show other than AMD diseases exist in the fundus image. FP are False Positive values, which mean that image is not AMD but it is detected as AMD, FN are False Negative values, which mean that image is AMD but it is not detected as AMD.

4.4 Results and Discussion

The proposed method is performed using different evaluation metrics such as accuracy (Acc), sensitivity (Sn), specificity (Sp), positive predicted value (PPV), and F1 score ($F1$). A total of 1349 retinal fundus images are used using four different databases. The evaluation of the proposed algorithm is performed for the detection of the macula. The results of our proposed method are also compared with some existing methods for each dataset to check superiority and effectiveness. Each experiment is replicated 5 times and their average results are taken. Table 2 displayed the results of macula detection using different datasets. The ophthalmologist manually marks the macula in each image to see the result of the macular detection. The macula segmented manually by a human observer is used as a ground truth. DRIVE mainly has normal subjects and contains good quality images therefore the proposed method showed 100 % results. Although using other datasets, the accuracy of our proposed method is still above 97 %.

Database	**Number of Images**	**Correctly Detected**	**Accuracy (%)**
DRIVE	40	40	100
STARE	20	19	95
MESSIDOR	1 200	1 127	93.9
DIARETDB1	89	85	95.5
Total	**1 349**	**1 271**	**94.21**

Table 2. Results of macula detection

Tables 3, 4, 5 and 6 show the quantitative comparison of our proposed method with other existing methods for each dataset and it can perceive that the proposed method outperforms the other state-of-the-art methods even for a large dataset. Our proposed method has achieved high values of sensitivity, specificity, and accuracy as compared to other methods as highlighted in bold text. The reason for the improvement is the use of contrast enhancement algorithm, detailed modified Kirsch's template feature for the segmentation, and spatial gradient-based edge detection feature which are not used by other authors. The detection of the macula is much

Authors	**Sensitivity (SN)**	**Specificity (SP)**	**Accuracy (ACC)**	**Time (s)**
GeethaRamani et al. [20]	–	–	90.0 %	N.A.
Dhivyaa et al. [43]	85.2 %	90.01 %	92.0 %	N.A.
Nugroho et al. [44]	86.5 %	85 %	93.01 %	N.A.
Guo et al. [45]	90 %	95.1 %	94 %	N.A.
Taori et al. [46]	75.5 %	89 %	92.5 %	N.A.
Maqsood et al. [47]	94.96 %	95.11 %	95.04 %	16.01
Our Proposed Method	**96.10 %**	**95.76 %**	**95.45 %**	15.89

Table 3. Performance comparison for STARE dataset. N.A. – data not provided.

Authors	**Sensitivity (SN)**	**Specificity (SP)**	**(ACC) (ACC)**	**Time (s)**
Pachade et al. [23]	68.2 %	75 %	92.8 %	N.A.
Kaya et al. [25]	–	–	97.5 %	N.A.
Jebaseeli et al. [48]	68.03 %	93.43 %	93.01 %	N.A.
Hidayatullah et al. [49]	–	–	94.07 %	N.A.
Our Proposed Method	**97.91 %**	**97.83 %**	**97.88 %**	15.31

Table 4. Performance comparison for DRIVE dataset. N.A. – data not provided.

better than existing methods for both the normal and AMD eyes because of the proper modeling of the macula rather than just detecting the dark region from the retinal fundus image.

Table 3 presents the comparison with STARE the dataset. The recorded results show a better performance of our proposed method while comparing it with existing methods. Table 4 shows the comparison in the context of the DRIVE dataset where the proposed method reveals enhanced performance and outperformed other methods quantitatively and is able to detect macula on 100 % of the images. Table 5 shows the comparison with the MESSIDOR dataset where our proposed method still shows enriched performance as compared to other ones. Table 6 shows the

Authors	**Sensitivity (SN)**	**Specificity (SP)**	**Accuracy (ACC)**	**Time (s)**
Tobin et al. [50]	–	–	76 %	N.A.
Deepak et al. [51]	95 %	90	99 %	N.A.
Akram et al. [52]	–	–	97.2 %	N.A.
Singh et al. [53]	94.68 %	97.19 %	95.47 %	N.A.
Gonzalo et al. [54]	92 %	92.1 %	-	N.A.
Li et al. [55]	70.8 %	–	91.2 %	N.A.
Yaqoob et al. [56]	–	–	89.89 %	22.2
Our Proposed Method	**98.93 %**	**99.46 %**	**99.2 %**	15.42

Table 5. Performance comparison for MESSIDOR dataset. N.A. – data not provided.

Authors	Sensitivity (SN)	Specificity (SP)	Accuracy (ACC)	Time (s)
Syed et al. [18]	96.42 %	80 %	97.5 %	N.A.
Ranamuka et al. [57]	75.43 %	90.9 %	95.84 %	N.A.
Patil et al. [58]	**99 %**	–	–	N.A.
Our Proposed Method	98.22 %	**97.54 %**	**97.86 %**	15.19

Table 6. Performance comparison for DIARETDB1 dataset. N.A. – data not provided.

comparison in the context of the DIARETDB1 dataset where our proposed method still exhibits better performance in view of the existing algorithms. Overall by comparison the proposed method exhibits improved performance towards the detection of the macula. The proposed method can be used for real-time evaluation and help the ophthalmologists in automated retinal image analysis.

The performance of our proposed method is also demonstrated using Confusion Matrix and ROC curves. The confusion matrix of STARE, DRIVE, MESSIDOR, and DIARETDB1 databases is shown in Figure 19. AUC is also a main quantitative metric that is acquired from ROC curves. The ROC curves plot against the false-positive rates (1-specificity) and true positive rate (sensitivity) by controlling the threshold values of the acquired probability maps which are used to get the macula. AUC computations are evaluated for the STARE, DRIVE, MESSIDOR, and DIARETDB1 databases. The ROC curve plot is shown in Figure 17.

Grading results of macula detection (with 95 % confidence intervals) are presented in Table 7 that displays data from the aforementioned databases (STARE, DRIVE, MESSIDOR, and DIARETDB1). The proposed method gives PPV, $F1$ and AUC of 94.67 %, 95.37 % and 95.76 % on STARE, 97.84 %, 97.86 % and 96.32 % on DRIVE, 99.47 %, 99.18 % and 97.83 % on MESSIDOR and 97.54 %, 97.86 % and 97.95 % on DIARETDB1 databases, respectively. The results are summarized in Figure 18.

Database	Sensitivity (%)	Specificity (%)	Accuracy (%)	F1 (%)	AUC (%)
STARE	96.10 (96.05–96.15)	95.76 (95.75–95.77)	95.45 (95.43–95.47)	95.37 (95.36–95.38)	95.76 (95.73–95.78)
DRIVE	97.91 (97.90–97.92)	97.83 (97.82–97.84)	97.88 (97.86–97.89)	97.86 (97.85–97.87)	96.32 (96.31–96.33)
MESSIDOR	98.93 (98.90–98.95)	99.46 (99.43–99.46)	99.2 (99.18–99.20)	99.18 (99.17–99.19)	97.83 (97.81–97.83)
DIARETDB1	98.22 (98.21–98.23)	97.54 (97.52–97.55)	97.86 (97.83–97.89)	97.86 (97.85–97.87)	97.95 (97.94–97.96)

Table 7. Macula detection results with 95 % confidence interval (CI)

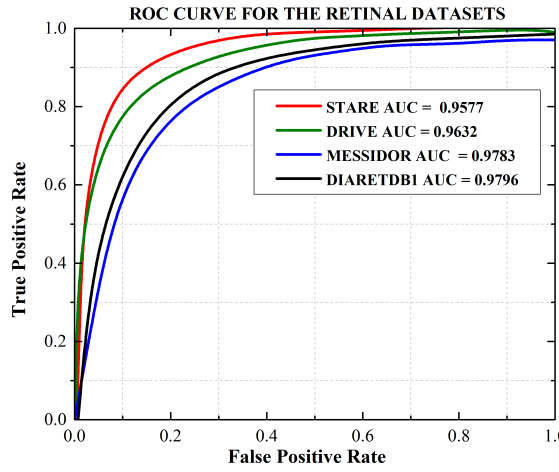

Figure 17. Receiver operating characteristic (ROC) plot for retinal STARE, DRIVE, MESSIDOR, and DIARETDB1 datasets

4.5 Computational Efficiency

Tables 3 to 6 show the time execution (in seconds) for each dataset image. Previous methods have failed to provide the computational efficiency of their proposed approaches. The results displayed in Tables 3 to 6 reveal that the execution of our proposed method takes 15.89 s for STARE, 15.31 s for DRIVE, 15.42 s for MESSIDOR, 15.19 s for DIARETDB1 databases. Since our main aim is to enhance the visualization to detect the macula, the minimization of the execution time will further be improved in future work.

5 CONCLUSION

Detection of macula and blood vessel segmentation has increased importance in present-day healthcare institutions. Various macula detection methods have been presented to extract their localization that is used to improve the medical analysis. However, these methods have numerous shortcomings, such as poor contrast when recognizing the retinal vessels, low segmentation of the retinal vessel due to inadequate noise, and blurring effect near the strong edges during the localization of the macula. This paper aimed to resolve the aforesaid concerns and proposed a new automatic detection and localization of macula by using shape-based feature recognition. Firstly, the input image is preprocessed using the NMHE histogram equalization approach and top-hat filter for the enhancement of dark regions and

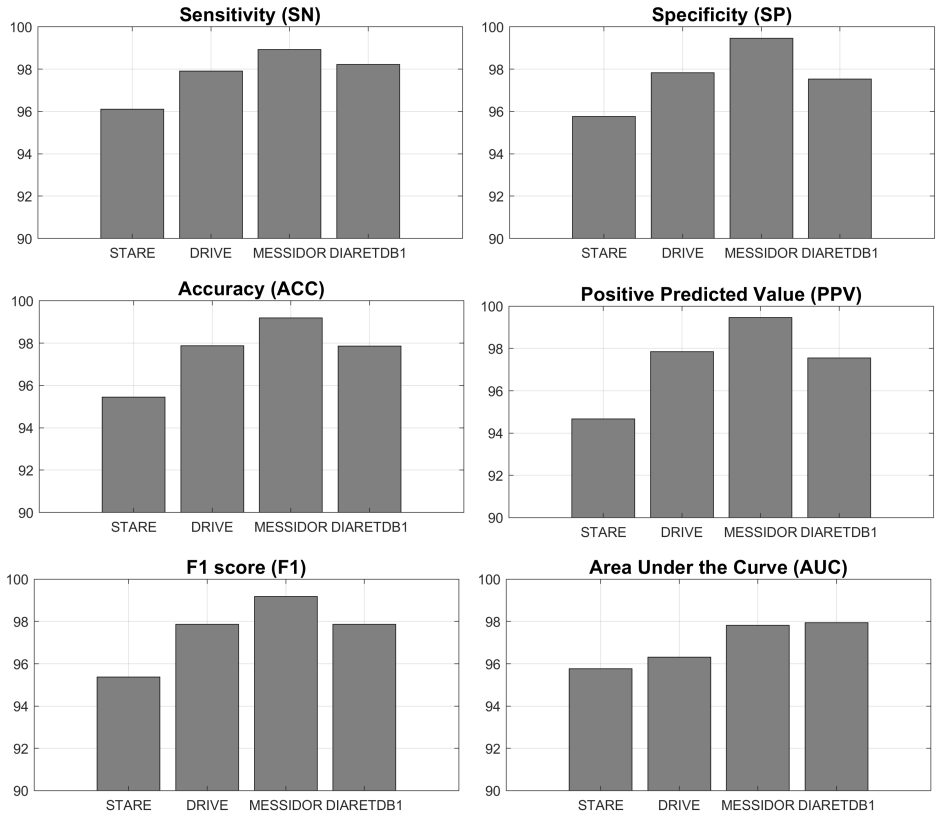

Figure 18. Summary of the performance measures of the proposed method on STARE, DRIVE, MESSIDOR, and DIARETDB1 datasets

subtraction from the modification to the legacy Kirsch's template method in the retinal fundus image. The modified Kirsch's template method is employed on the contrast-enhanced image to filter and enhance the blood vessels. The OTSU thresholding is employed for the segmentation of the dark regions. The background and black region estimated image are subtracted from each other to get the macula. A detailed feature vector for each candidate region is formed consisting of four types of features such as eccentricity, diameter, radius, and statistical-based features. Based on these features the macula is detected and recognized. The proposed method was applied to 1349 images from the STARE, DRIVE, MESSIDOR, and DIARETDB1 datasets, and achieved an accuracy of 95.45 %, 97.88 %, 99.20 %, and 97.86 %, respectively. Moreover our proposed method provides visually pleasant and high-quality results and is more efficient for the automatic detection of macula and outperformed other methods. The macula is detected accurately with less amount

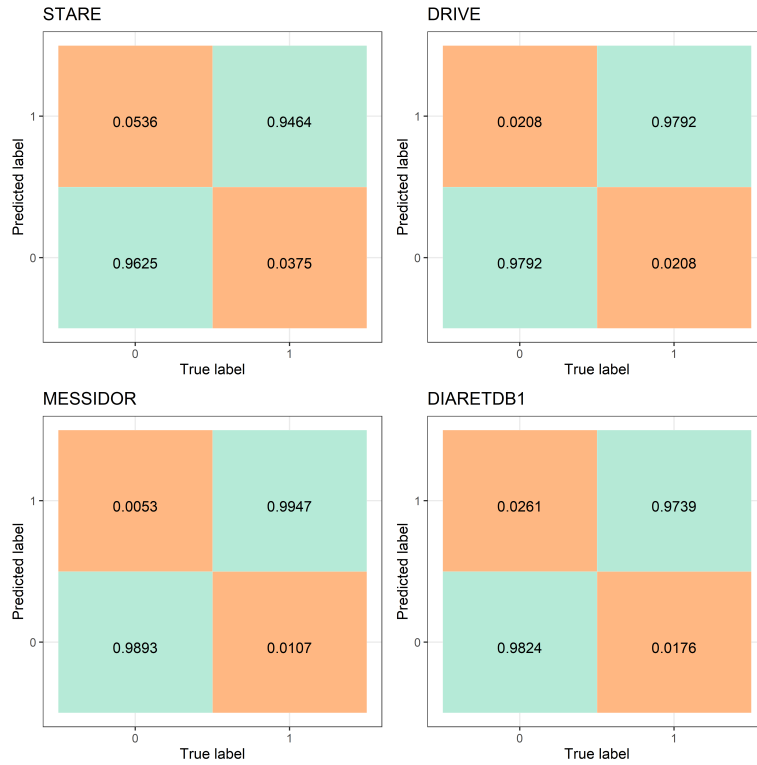

Figure 19. Confusion matrices for classification on retinal STARE, DRIVE, MESSIDOR, and DIARETDB1 datasets

of computation time and produces superior results for both the healthy and diseased eye.

In the future, the proposed method will be further analyzed for other application areas of biomedical image processing.

REFERENCES

[1] Flaxman, S. R.—Bourne, R. R. A.—Resnikoff, S.—Ackland, P.—Braithwaite, T. et al.: Global Causes of Blindness and Distance Vision Impairment 1990–2020: A Systematic Review and Meta-Analysis. The Lancet Global Health, Vol. 5, 2017, No. 12, pp. 1221–1234, doi: 10.1016/S2214-109X(17)30393-5.

[2] Acharya, U. U.—Mookiah, M. R. K.—Koh, J. E. W.—Tan, J. H.—Noronha, K.—Bhandary, S. V.—Rao, A. K.—Hagiwara, Y.—Chua, C. K.—Laude, A.: Novel Risk Index for the Identification of Age-Related Macular

Degeneration Using Radon Transform and DWT Features. Computers in Biology and Medicine, Vol. 73, 2016, pp. 131–140, doi: 10.1016/j.compbiomed.2016.04.009.

[3] Tan, J. H.—Bhandary, S. V.—Sivaprasad, S.—Hagiwara, Y.—Bagchi, A.—Raghavendra, U.—Rao, A. K.—Raju, B.—Shetty, N. S.—Gertych, A.—Chua, K. C.—Acharya, U. R.: Age-Related Macular Degeneration Detection Using Deep Convolutional Neural Network. Future Generation Computer Systems, Vol. 87, 2018, pp. 127–135, doi: 10.1016/j.future.2018.05.001.

[4] Mathews, D. R.—Stratton, I. M.—Aldington, S. J.—Holman, R. M.—Kohner, E. M.: Risks of Progression of Retinopathy and Vision Loss Related to Tight Blood Pressure Control in Type 2 Diabetes Mellitus: UKPDS 60. Archives of Ophthalmology, Vol. 122, 2004, No. 11, pp. 1631–1640, doi: 10.1001/archopht.122.11.1631.

[5] Delcourt, C.—Massin, P.—Rosilio, M.: Epidemiology of Diabetic Retinopathy: Expected vs Reported Prevalence of Cases in the French Population. Diabetes and Metabolism, Vol. 35, 2019, No. 6, pp. 431–438, doi: 10.1016/j.diabet.2009.06.002.

[6] Kanagasingam, Y.—Bhuiyan, A.—Abramoff, M. D.—Smith, R. T.—Goldschmidt, L.—Wong, T. Y.: Progress on Retinal Image Analysis for Age Related Macular Degeneration. Progress in Retinal and Eye Research, Vol. 38, 2014, pp. 20–42, doi: 10.1016/j.preteyeres.2013.10.002.

[7] Maqsood, S.—Javed, U.: Multi-Modal Medical Image Fusion Based on Two-Scale Image Decomposition and Sparse Representation. Biomedical Signal Processing and Control, Vol. 57, 2020, Art. No. 101810, doi: 10.1016/j.bspc.2019.101810.

[8] Muzammil, S. R.—Maqsood, S.—Haider, S.—Damaševičius, R.: CSID: A Novel Multimodal Image Fusion Algorithm for Enhanced Clinical Diagnosis. Diagnostics, Vol. 10, 2020, No. 11, Art. No. 904, doi: 10.3390/diagnostics10110904.

[9] Resnikoff, S.—Felch, W.—Gauthier, T.-M—Spivey, B.: The Number of Ophthalmologists in Practice and Training Worldwide: A Growing Gap Despite More Than 200 000 Practitioners. British Journal of Ophthalmology, Vol. 96, 2012, No. 6, pp. 783–787, doi: 10.1136/bjophthalmol-2011-301378.

[10] Roesch, K.—Swedish, T.—Raskar, R.: Automated Retinal Imaging and Trend Analysis – A Tool for Health Monitoring. Clinical Ophthalmology, Vol. 11, 2017, pp. 1015–1020, doi: 10.2147/OPTH.S116265.

[11] Schmidt-Erfurth, U.—Sadeghipour, A.—Gerendas, B. S.—Waldstein, S. M.—Bogunović, H.: Artificial Intelligence in Retina. Progress in Retinal and Eye Research, Vol. 67, 2018, pp. 1–29, doi: 10.1016/j.preteyeres.2018.07.004.

[12] Abràmoff, M. D.—Garvin, M. K.—Sonka, M.: Retinal Imaging and Image Analysis. IEEE Reviews in Biomedical Engineering, Vol. 3, 2010, pp. 169–208, doi: 10.1109/RBME.2010.2084567.

[13] Hood, D. C.—Raza, A. S.—de Moraes, C. G. V—Liebmann, J. M.—Ritch, R.: Glaucomatous Damage of the Macula. Progress in Retinal and Eye Research, Vol. 32, 2013, pp. 1–21, doi: 10.1016/j.preteyeres.2012.08.003.

[14] Ciulla, T. A.—Amador, A. G.—Zinman, B.: Diabetic Retinopathy and Diabetic Macular Edema: Pathophysiology, Screening, and Novel Therapies. Diabetes Care, Vol. 26, 2003, No. 9, pp. 2653–2664, doi: 10.2337/diacare.26.9.2653.

[15] Alais, R.—Dokládal, P.—Erginay, A.—Figliuzzi, B.—Decencière, E.: Fast Macula Detection and Application to Retinal Image Quality Assessment. Biomedical Signal Processing and Control, Vol. 55, 2020, Art. No. 101567, doi: 10.1016/j.bspc.2019.101567.

[16] Ramasamy, L. K.—Padinjappurathu, S. G.—Kadry, S.—Damaševičius, R.: Detection of Diabetic Retinopathy Using a Fusion of Textural and Ridgelet Features of Retinal Images and Sequential Minimal Optimization Classifier. PeerJ Computer Science, Vol. 7, 2021, Art. No. e456, doi: 10.7717/peerj-cs.456.

[17] Decencière, E.—Cazuguel, G.—Zhang, X.—Thibault, G.—Klein, J.-C.—Meyer, F. et al.: TeleOphta: Machine Learning and Image Processing Methods for Teleophthalmology. IRBM, Vol. 34, 2013, No. 2, pp. 196–203, doi: 10.1016/j.irbm.2013.01.010.

[18] Syed, A. M.—Akram, M. U.—Akram, T.—Muzammal, M.—Khalid, S.—Khan, M. A.: Fundus Images-Based Detection and Grading of Macular Edema Using Robust Macula Localization. IEEE Access, Vol. 6, 2018, pp. 58784–58793, doi: 10.1109/ACCESS.2018.2873415.

[19] Nazari, A.—Mustafa, M. M.—Zulkifley, M. A.: Segmentation of Retinal Blood Vessels by Top-Hat Multi-Scale Detection for Optic Disc Removal. Jurnal Teknologi, Vol. 77, 2015, No. 6, pp. 47–53, doi: 10.11113/jt.v77.6226.

[20] GeethaRamani, R.—Balasubramanian, L.: Macula Segmentation and Fovea Localization Employing Image Processing and Heuristic Based Clustering for Automated Retinal Screening. Computer Methods and Programs in Biomedicine, Vol. 160, 2018, pp. 153–163, doi: 10.1016/j.cmpb.2018.03.020.

[21] Orujov, F.—Maskeliūnas, R.—Damaševičius, R.—Wei, W.: Fuzzy Based Image Edge Detection Algorithm for Blood Vessel Detection in Retinal Images. Applied Soft Computing, Vol. 94, 2020, Art. No. 106452, doi: 10.1016/j.asoc.2020.106452.

[22] Saroj, S. K.—Kumar, R.—Singh, N. P.: Fréchet PDF Based Matched Filter Approach for Retinal Blood Vessels Segmentation. Computer Methods and Programs in Biomedicine, Vol. 194, 2020, Art. No. 105490, doi: 10.1016/j.cmpb.2020.105490.

[23] Ghoshal, R.—Saha, A.—Das, S.: An Improved Vessel Extraction Scheme from Retinal Fundus Images. Multimedia Tools and Applications, Vol. 78, 2019, No. 18, pp. 25221–25239, doi: 10.1007/s11042-019-7719-9.

[24] Dharmawan, D. A.—Ng, B. P.—Rahardja, S.: A New Optic Disc Segmentation Method Using a Modified Dolph-Chebyshev Matched Filter. Biomedical Signal Processing and Control, Vol. 59, 2020, Art. No. 101932, doi: 10.1016/j.bspc.2020.101932.

[25] Kaya, Y.: A Novel Method for Optic Disc Detection in Retinal Images Using the Cuckoo Search Algorithm and Structural Similarity Index. Multimedia Tools and Applications, Vol. 79, 2020, No. 31–32, pp. 23387–23400, doi: 10.1007/s11042-020-09080-5.

[26] Palanivel, D. A.—Natarajan, S.—Gopalakrishnan, S.: Retinal Vessel Segmentation Using Multifractal Characterization. Applied Soft Computing, Vol. 94, 2020, Art. No. 106439, doi: 10.1016/j.asoc.2020.106439.

[27] Kadry, S.—Rajinikanth, V.—Damaševičius, R.—Taniar, D.: Retinal Vessel Segmentation with Slime-Mould-Optimization Based Multi-Scale-Matched-Filter. 2021 IEEE 7th International Conference on Bio Signals, Images and Instrumentation (ICBSII 2021), 2021, pp. 1–5, doi: 10.1109/ICBSII51839.2021.9445135.

[28] Agurto, C.—Murray, V.—Yu, H.—Wigdahl, J.—Pattichis, M.—Nemeth, S.—Barriga, E. S.—Soliz, P.: A Multiscale Optimization Approach to Detect Exudates in the Macula. IEEE Journal of Biomedical and Health Informatics, Vol. 18, 2014, No. 4, pp. 1328–1336, doi: 10.1109/JBHI.2013.2296399.

[29] Aljazaeri, M.—Bazi, Y.—AlMubarak, H.—Alajlan, N.: Faster R-CNN and DenseNet Regression for Glaucoma Detection in Retinal Fundus Images. 2020 2nd International Conference on Computer and Information Sciences (ICCIS), 2020, pp. 1–4, doi: 10.1109/ICCIS49240.2020.9257680.

[30] Poddar, S.—Tewary, S.—Sharma, D.—Karar, V.—Ghosh, A.—Pal, S. K.: Non-Parametric Modified Histogram Equalisation for Contrast Enhancement. IET Image Processing, Vol. 7, 2013, No. 7, pp. 641–652, doi: 10.1049/iet-ipr.2012.0507.

[31] Dash, J.—Bhoi, N.: Retinal Blood Vessel Extraction Using Morphological Operators and Kirsch's Template. In: Wang, J., Reddy, G., Prasad, V., Reddy, V. (Eds.): Soft Computing and Signal Processing. Springer, Singapore, Advances in Intelligent Systems and Computing, Vol. 900, 2019, pp. 603–611, doi: 10.1007/978-981-13-3600-3_57.

[32] Krestanova, A.—Kubicek, J.—Penhaker, M.: Recent Techniques and Trends for Retinal Blood Vessel Extraction and Tortuosity Evaluation: A Comprehensive Review. IEEE Access, Vol. 8, 2020, pp. 197787–197816, doi: 10.1109/ACCESS.2020.3033027.

[33] Hou, S.—Sun, Z.—Yang, L.—Song, Y.: Kirsch Direction Template Despeckling Algorithm of High-Resolution SAR Images-Based on Structural Information Detection. IEEE Geoscience and Remote Sensing Letters, Vol. 18, 2021, No. 1, pp. 177–181, doi: 10.1109/LGRS.2020.2966369.

[34] Maqsood, S.—Javed, U.—Riaz, M. R.—Muzammil, M.—Muhammad, F.—Kim, S.: Multiscale Image Matting Based Multi-Focus Image Fusion Technique. Electronics, Vol. 9, 2020, No. 3, Art. No. 472, doi: 10.3390/electronics9030472.

[35] Dhivyaa, C. R.—Vijayakumar, M.: An Effective Detection Mechanism for Localizing Macular Region and Grading Maculopathy. Journal of Medical Systems, Vol. 43, 2019, No. 3, Art. No. 53, doi: 10.1007/s10916-019-1163-2.

[36] Gabryel, M.—Damaševičius, R.: The Image Classification with Different Types of Image Features. In: Rutkowski, L., Korytkowski, M., Scherer, R., Tadeusiewicz, R., Zadeh, L., Zurada, J. (Eds.): International Conference on Artificial Intelligence and Soft Computing (ICAISC 2017). Springer, Cham, Lecture Notes in Computer Science, Vol. 10245, 2017, pp. 497–506, doi: 10.1007/978-3-319-59063-9_44.

[37] He, Y.—Liu, P.—Wang, Z.—Hu, Z.—Yang, Y.: Filter Pruning via Geometric Median for Deep Convolutional Neural Networks Acceleration. 2019 IEEE/CVF Conference on Computer Vision and Pattern Recognition (CVPR), 2019, pp. 4335–4344, doi: 10.1109/cvpr.2019.00447.

[38] Du, H.—Chen, X.—Xi, J.: An Improved Background Segmentation Algorithm for Fringe Projection Profilometry Based on Otsu Method. Optics Communications, Vol. 453, 2019, Art. No. 124206, doi: 10.1016/j.optcom.2019.06.044.

[39] Staal, J.—Abràmoff, M. M.—Niemeijer, M.—Viergever, M. A.—van Ginneken, B.: Ridge-Based Vessel Segmentation in Color Images of the Retina. IEEE Transactions on Medical Imaging, Vol. 23, 2004, No. 4, pp. 501–509, doi: 10.1109/TMI.2004.825627.

[40] Goldbaum, M.: Structured Analysis of the Retina. 2013. Available at: `https://cecas.clemson.edu/~ahoover/stare/` [20 October 2021].

[41] Decencière, E.—Zhang, X.—Cazuguel, G.—Lay, B.—Cochener, B.—Trone, C.—Gain, P.—Ordonez, R.—Massin, P.—Erginay, A.—Charton, B.—Klein, J.-C.: Feedback on a Publicly Distributed Image Database: The Messidor Database. Image Analysis and Stereology, Vol. 33, 2014, No. 3, pp. 231–234, doi: 10.5566/ias.1155.

[42] Kauppi, T.—Kalesnykiene, V.—Kamarainen, J.-K.—Lensu, L.—Sorri, I.—Raninen, A.—Voutilainen, R.—Uusitalo, H.—Kälviäinen, H.—Pietilä, J.: DIARETDB1 Diabetic Retinopathy Database and Evaluation Protocol. In: Zwiggelaar, R., Labrosse, F. (Eds.): Medical Image Understanding and Analysis 2007. British Machine Vision Association (BMVA), 2007, pp. 61–65, doi: 10.5244/c.21.15.

[43] Dhivyaa, C. R.—Vijayakumar, M.: The Blood Vasculature of the Retina Using Routine Segmentation. IETE Journal of Research, 2020, pp. 1–9, doi: 10.1080/03772063.2020.1725664.

[44] Nugroho, H. A.—Listyalina, L.—Wibirama, S.—Oktoeberza, W. K.: Automated Determination of Macula Centre Point Based on Geometrical and Pixel Value Approaches to Support Detection of Foveal Avascular Zone. International Journal of Innovative Computing, Information and Control, Vol. 14, 2018, No. 4, pp. 1453–1463, doi: 10.24507/ijicic.14.04.1453.

[45] Guo, X.—Li, Q.—Sun, C.—Lu, Y. N.: Automatic Localization of Macular Area Based on Structure Label Transfer. International Journal of Ophthalmology, Vol. 11, 2018, No. 3, pp. 422–428, doi: 10.18240/ijo.2018.03.12.

[46] Taori, A. M.—Chaudhari, A. K.—Patankar, S. S.—Kulkarni, J. V.: Segmentation of Macula in Retinal Images Using Automated Seeding Region Growing Technique. 2016 International Conference on Inventive Computation Technologies (ICICT), 2016, pp. 1–5, doi: 10.1109/INVENTIVE.2016.7824792.

[47] Maqsood, S.—Damaševičius, R.—Maskeliūnas, R.: Hemorrhage Detection Based on 3D CNN Deep Learning Framework and Feature Fusion for Evaluating Retinal Abnormality in Diabetic Patients. Sensors, Vol. 21, 2021, No. 11, Art. No. 3865, doi: 10.3390/s21113865.

[48] Kaur, S.—Mann, K. S.: Optimized Technique for Detection of Diabetic Retinopathy Using Segmented Retinal Blood Vessels. 2019 International Conference on Automation, Computational and Technology Management (ICACTM), 2019, pp. 79–83, doi: 10.1109/ICACTM.2019.8776708.

[49] Aguirre-Ramos, H.—Avina-Cervantes, J. G.—Cruz-Aceves, I.—Ruiz-Pinales, J.—Ledesma, S.: Blood Vessel Segmentation in Retinal Fundus Images Using Gabor Filters, Fractional Derivatives, and Expectation Maximization. Applied Mathematics and Computation, Vol. 339, 2018, pp. 568–587, doi: 10.1016/j.amc.2018.07.057.

[50] Tobin, K. W.—Chaum, E.—Govindasamy, V. P.—Karnowski, T. P.: Detection of Anatomic Structures in Human Retinal Imagery. IEEE Transactions on Medical Imaging, Vol. 26, 2007, No. 12, pp. 1729–1739, doi: 10.1109/tmi.2007.902801.

[51] Deepak, K. S.—Medathati, N. V. K.—Sivaswamy, J.: Detection and Discrimination of Disease-Related Abnormalities Based on Learning Normal Cases. Pattern Recognition, Vol. 45, 2012, No. 10, pp. 3707–3716, doi: 10.1016/j.patcog.2012.03.020.

[52] Akram, M. U.—Tariq, A.—Khan, S. A.—Javed, M. Y.: Automated Detection of Exudates and Macula for Grading of Diabetic Macular Edema. Computer Methods and Programs in Biomedicine, Vol. 114, 2014, No. 2, pp. 141–152, doi: 10.1016/j.cmpb.2014.01.010.

[53] Singh, R. K.—Gorantla, R.: DMENet: Diabetic Macular Edema Diagnosis Using Hierarchical Ensemble of CNNs. PLoS ONE, Vol. 15, 2020, No. 2, Art. No. e0220677, doi: 10.1371/journal.pone.0220677.

[54] Gozáles-Gonzalo, C.—Sánchez-Gutiérrez, V.—Hernández-Martinez, P.—Contreras, I.—Lechanteur, Y. T.—Domanian, A.—van Ginneken, B.—Sanchez, C. I.: Evaluation of a Deep Learning System for the Joint Automated Detection of Diabetic Retinopathy and Age-Related Macular Degeneration. Acta Ophthalmologica, Vol. 98, 2020, No. 4, pp. 368–377, doi: 10.1111/aos.14306.

[55] Li, X.—Hu, X.—Yu, L.—Zhu, L.—Fu, C. W.—Heng, P. A.: CANet: Cross-Disease Attention Network for Joint Diabetic Retinopathy and Diabetic Macular Edema Grading. IEEE Transcations on Medical Imaging, Vol. 39, 2020, No. 5, pp. 1483–1493, doi: 10.1109/tmi.2019.2951844.

[56] Yaqoob, M. K.—Ali, S. F.—Kareem, I.—Fraz, M. M.: Feature-Based Optimized Deep Residual Network Architecture for Diabetic Retinopathy Detection. 2020 IEEE 23rd International Multitopic Conference (INMIC), pp. 1–6, 2020, doi: 10.1109/inmic50486.2020.9318096.

[57] Ranamuka, N. G.—Meegama, R. G. N.: Detection of Hard Exudates from Diabetic Retinopathy Images Using Fuzzy Logic. IET Image Processing, Vol. 7, 2013, No. 2, pp. 121–130, doi: 10.1049/iet-ipr.2012.0134.

[58] Patil, S. B.—Patil, B. P.: Automated Macula Proximity Diagnosis for Early Finding of Diabetic Macular Edema. Research on Biomedical Engineering, Vol. 36, 2020, pp. 249–265, doi: 10.1007/s42600-020-00065-9.

Sarmad Maqsood received his B.Sc. and M.Sc. degrees in electronic engineering from the International Islamic University, Islamabad, Pakistan, in 2015 and 2018, respectively. He is currently Ph.D. student at the Department of Software Engineering, Kaunas University of Technology, Lithuania. His research interests are image processing, medical image analysis, multimodal data fusion and deep learning methods. He is the author of 8 research articles.

Robertas Damaševičius received his Ph.D. degree in informatics engineering from the Kaunas University of Technology, Lithuania, in 2005. He is currently Professor with the Department of Software Engineering, Kaunas University of Technology, Lithuania, and Adjunct Professor with the Faculty of Applied Mathematics, Silesian University of Technology, Poland. His research interests include sustainable software engineering, human–computer interfaces, and assisted living. He is the author of more than 380 articles. He is the Editor-in-Chief of the Information Technology and Control Journal. He is Associated Editor of PLoS One, IET Image Processing, International Journal of Imaging Systems and Technology (IMA), and Academic Editor of PeerJ Computer Science Journal.

Faisal Mehmood Shah received his B.Sc. degree in electronics engineering from the Islamabad, Pakistan, in 2015, and the M.Sc. degree in electrical engineering from the North China Electric Power University, Beijing, China, in 2018. His main research interests include high-frequency HVDC converters and power conversion system for renewable energy nano grid, power conversion, and control.

Rytis Maskeliūnas received his Ph.D. degree in computer science, in 2009. He is currently Invited Professor with the Department of Faculty of Applied Mathematics, Silesian University of Technology, Gliwice, Poland. He is the author of more than 120 articles and serves as reviewer for various refereed journals. His main areas of research are multimodal signal processing, development of multimodal interfaces targeted at elderly and people with disabilities. He has won various awards/honors, including Best Young Scientist Award of 2012, National Science Academy Award for Young Scholars of Lithuania in 2010, etc.